

CAPTURE EFFICIENCY OF MAGNETICALLY LABELED PARTICLES TRAVELING THROUGH AN INTRACRANIAL ANEURYSM

M. CARDONA* and J.RAMÍREZ

Department of Mechanical Engineering, Universidad Nacional de Colombia, Sede Medellín, COLOMBIA
E-mail: mecardonata@unal.edu.co

A.G. BENAVIDES-MORAN

Department of Mechanical and Mechatronics Engineering, Universidad Nacional de Colombia
Sede Bogotá, COLOMBIA

Cell manipulation using external magnetic fields has been proposed to accelerate the neck reendothelization of saccular unruptured stented intracranial aneurysms. This work presents a computational fluid dynamics (CFD) model of a Saccular Brain Aneurysm that incorporates a helicoidal stent. An Eulerian-Lagrangian model implemented in ANSYS-Fluent is used to simulate the hemodynamics in the aneurysm. In silico studies have been conducted to describe the incidence of the magnetic field direction, frequency and amplitude on the blood hemodynamics and particle capture efficiency, when an external magnetic field is used to trap magnetically labeled particles traveling through the aneurysm. It is found that the magnetic field direction affects the particle concentration in the target region. Simulation results show that the highest particle capture efficiency is obtained with a 1T magnetic field amplitude in an open bore MRI scanner, when a permanent magnet is used.

Key words: endothelization, particle manipulation, computational fluid dynamics, magnetohydrodynamics.

1. Introduction

Brain Aneurysm or Intracranial Aneurysm (IA) are pathological localized dilatations resulting from a weakness in the cerebrovascular wall in direct communication with the lumen and blood flow [1]. According to the Brain Aneurysm Foundation [2] almost 500,000 deaths worldwide each year are caused by brain aneurysms and half the victims are younger than 50 years old.

Besides surgical management, flow diversion has emerged as the main treatment for a wide neck saccular brain aneurysm located in the anterior communication artery (ACoA) in circle of Willis [1, 3]. Being a minimally invasive treatment, flow diverters (FDs) promote aneurysm occlusion by acting as a scaffold for a controlled thrombosis formation in the aneurysm ostium surface.

The ability of the tissue to occlude the neck depends on the migration of surrounding mature endothelial cells and the attraction and adhesion of circulating endothelial progenitor cells (EPCs) to the ostium region. Shear stress preconditioning has been suggested as a feasible option to improve the functioning of EPCs to be seeded onto the tissue-engineered vascular constructs [4]. However, to avoid thrombotic complications, such as late stent thrombosis, it is required to accelerate re-endothelialization processes [5].

Providing magnetic features to living cells has been previously proposed as an efficient mechanism to accelerate capture of EPCs [6, 7]. The essential element in achieving that is to add magnetic nanoparticles (MNP) to the cells and then drive the modified cells to target regions using external magnetic fields [8, 9]. This magnetic manipulation allows acceleration of the afore mentioned re-endothelialization process and seeks to avoid further clinical interventions [10].

* To whom correspondence should be addressed

Permanent magnets or electromagnetic field sources can be used to generate an efficient external magnetic field for cell capturing. As recently presented by Connell *et al.* [7], magnetic field gradients, inherent to all magnetic resonance imaging (MRI) systems, are used to steer ferromagnetic particles to a target region in a process called magnetic resonance targeting.

Under flow conditions, particle trapping occurs if the magnetic field pulls the particle out of the strong center-line flow, before it leaves the region of interest. This phenomenon is maximum when a magnetic field is perpendicular to the particle trajectory [11]. In a one-way interaction, particles have the same velocity field as the fluid, in this sense, to study the behavior of particles traveling inside an IA, the particle velocity can be calculated using a hemodynamic approach. It is important to consider that aneurysm hemodynamics depends both on the morphological characteristics of the vessel and the existence of endovascular treatment [12].

It has been demonstrated that speeding up the capture of cells in blood flow, using external magnetic fields, depends on different aspects such as magnetic features, particle injection, flow patterns and particle characteristics [7]. The analysis of the *in vivo* behavior of the particles in blood flow is not as simple as comparing the magnetic forces on each particle with the forces predicted by Stokes drag models [13]. Conversely, it is a complex process that involves several interactions such as magnetic attraction, hemodynamic forces and Brownian forces.

To gain some insight into the cells location process, *in vitro* experiments and mathematical modelling are usually used; specially, *in silico* studies have been the key to understand how particles respond to various stimuli in a relatively short period of time, where computational fluid dynamics (CFD) is the most common numerical simulation technique used to estimate disturbances on the hemodynamic flow field due to external agents.

After understanding the particle manipulation process, the capture efficiency (CE) on endovascular treatment can be calculated as the fraction of inserted particles that is attracted by the magnetic field towards the vessel wall and are trapped on the stent struts [14]. Considering the available configurations for the imposed magnetic fields, it is important to study which magnetic field configuration increases CE, before the fabrication of any capture system.

Some effects over the magnetically labeled particle CE have been previously studied using numerical models. Bose & Banerjee [15] studied in a 2D computational simulation the influence of external non-uniform magnetic field strength, particle size, flow Reynolds number (Re), particle concentrations and particle loadings on the CE. They reported that a gradual increase in the CE is observed for large particle sizes and with the increment of the external magnetic field strength.

Using a mathematical model and *in vitro* experiments, Sharma *et al.* [16] found a direct relationship of the CE with the magnetic field strength and an inverse relation with particle inlet velocity. In their experimental study, Mirzababaei *et al.* [17] confirmed the aforementioned relationship between particle velocity and magnetic strength and indicated that aneurysm volume is an additional important parameter for the CE.

Beside the morphology of the aneurysm, the magnetic resonance (MR) scanner configuration implies a different magnetic field direction to the ostium. Cylindrical scanners have a magnetic field parallel to the caudocranial direction, meanwhile an open bore MR magnetic field is perpendicular to head feet [18]. *In vitro* experiments verified that magnetically labeled cells in the presence of a magnetic field could rapidly move toward the magnet [19]. In this sense, the direction of the particle trajectory can be manipulated by changing the MR scanner, entailing a change in the direction of the magnetic field.

Existing studies have focused on the influence of the magnetic field strength and the physiochemical properties of the particles [13, 14, 20-23]. It may be suggested that, in addition to the magnetic field strength, other magnetic field features are related to the increment of CE which, up until now, has not been thoroughly studied. The aim of this work is to study the influence of the strength, frequency and direction of the magnetic field over the particle targeting efficacy in an idealized saccular stented aneurysm geometry.

2. Formulation of the problem

To explore how EPCs are likely to respond to a magnetic targeting delivery in the stented wide neck aneurysmal model, *in silico* studies are performed. Blood flow and particle motion behavior due to the magnetic field are studied using the Euler-Lagrange approach after variations of the amplitude, frequency and direction of

the magnetic field. A discrete phase model is used to simulate magnetic label endothelial cells that are represented as particles injected in the blood. The number of trap particles is used to calculate the CE. A comparison of the obtained results is used to identify factors of incidence over magnetic configurations on the CE.

2.1. Magnetohydrodynamic

Blood is considered a Non-Newtonian and electrically conducting fluid [24]. According to Hagdel *et al.* [25] the Herschel-Bulkley model from Eq.(2.1) is the preferred dynamic viscosity model for the analysis of blood flow where η is the shear viscosity, when blood is exposed to a magnetic field. The consistency index is $k = 8.9721 \times 10^{-3} \text{Ns}^n / \text{m}^2$, the power-law index is $n = 0.8601$, and $\tau_0 = 0.0175 \text{N} / \text{m}^2$ is the yield stress threshold [26]:

$$\eta = k\dot{\gamma}^{n-1} + \left(\frac{\tau_0}{\dot{\gamma}} \right). \quad (2.1)$$

Magnetic effects in the flow are described using a magnetohydrodynamic (MHD) model. The Navier-Stokes equations are coupled with the magnetic induction equation derived from Ohm's law and Maxwell's equations [15, 27], where μ_0 is the magnetic permeability, \vec{J} is the current density, \vec{E} is the electric field and \vec{B} is the magnetic field:

$$\nabla \cdot \vec{B} = 0, \quad (2.2)$$

$$\nabla \times \vec{B} = \mu_0 \vec{J}, \quad (2.3)$$

$$\nabla \times \vec{E} = -\frac{\partial \vec{B}}{\partial t}. \quad (2.4)$$

According to the above mentioned considerations, the governing equations of flow for an incompressible, homogeneous, non-Newtonian biofluid couple the Navier-Stokes and Maxwell equations where both the electric conductivity (σ) and magnetization (\vec{M}) appear in the momentum equation source term as shown in Eq.(2.6).

The equation of continuity

$$\nabla \cdot \vec{V} = 0. \quad (2.5)$$

The equation of momentum

$$\frac{\partial \vec{V}}{\partial t} + (\vec{V} \cdot \nabla) \vec{V} = \mu \nabla^2 \vec{V} + \frac{1}{\rho} \left[-\nabla p + (\vec{J} \times \vec{B}) + \mu_0 (\vec{M} \cdot \nabla) \vec{H} \right] \quad (2.6)$$

where $\vec{J} = \sigma \vec{E}$.

The Lorentz force and the magnetization force are included in the momentum equation as body forces acting on the flow. The Lorentz force is created by electrical conductivity of the fluid moving through an imposed magnetic field and the magnetization force is generated due to the non-uniformity of the imposed magnetic field and leads to magnetization of the fluid.

2.2. Discrete phase model (DPM)

Labeled Cells with $29.8 \pm 0.1 \text{ pg}$ iron oxide/cell [23], are modeled as spherical particles with a mean diameter of $10 \mu\text{m}$, based on the mean endothelial cell width and length. Considering the total volume of the domain, $1.468 \times 10^{-6} \text{ m}^3$, the discrete phase is defined to be 1% of the total volume. With this consideration, the discrete phase volume fraction is negligible.

Blood is considered to be the continuous phase and one-way interaction is assumed with particle flow fields. Particle trajectories are obtained by integrating the particles equation of motion written in a Lagrangian framework. In general, forces affecting the particle motion include buoyancy, particle–fluid interaction forces, inertia, gravitational forces, thermal kinetic energy, Brownian motion and magnetostatic as an interparticle effect [28]. Considering the scale of the mentioned forces, this study considers only the magnetic force (F_m) and the viscous drag force (F_s) since their order of magnitude controls the particle motion [29]. In addition, particle-particle interaction is neglected as the particle flow is dilute.

2.3. Computational model

Geometry

As presented in Fig.1, an idealized 3D model of a saccular brain aneurysm of the ACoA with a curvature of 60° is reconstructed according to the most common location of the pathology [12, 30]. The geometry for the analysis has the dome-to-neck ratio lower than 1.5, defined for wide-neck aneurysms [1]. Both the perpendicular height and neck diameter are 5 mm and the aspect ratio (depth/neck width) is 1. The parent vessel diameter is set to 4 mm and to ensure that the flow profile is fully developed, the proximal section of the parent artery is set to 10D, resulting in a length L of 40 mm .

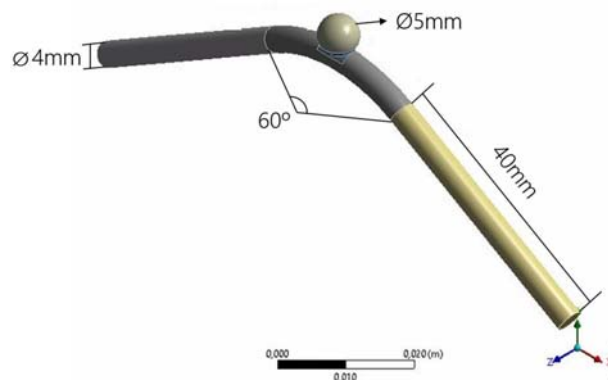


Fig.1. Idealized 3D model of a saccular brain aneurysm.

To characterize the hemodynamic modifications caused by endovascular treatments, a helicoidal stent with a rounded strut diameter of $70 \mu\text{m}$ is placed facing the ostium. As suggested by Bouillot *et al.* [31] the virtual stent is reduced to a patch across the IA neck as illustrated in Fig.2.

Computational simulations are performed in a work station computer, Intel® Xeon® E5-1650 v2 Processor, Six Core HT, 3.5 GHz Turbo, 64GB RAM memory using the commercial CFD software ANSYS FLUENT version 15.0 [32]. A high resolution computational unstructured mesh composed of tetrahedrons is created. Mesh-independent analysis is performed comparing the wall shear stress (WSS) in the middle point of the stent wall, resulting in a tetrahedral mesh of 2.6 million element mesh, with 0.84 as a maximum skewness for the whole domain. Results of the analysis are presented in Table 1.

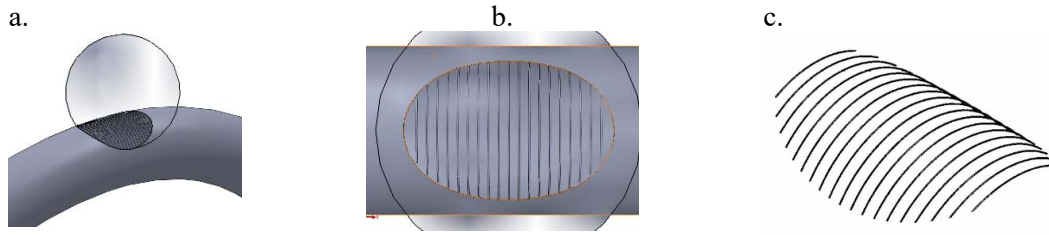


Fig.2. Helical virtual stent patch in saccular aneurysm neck: a. aneurysm 3D view; b. ostium bottom view; c. stent isometric view.

Table 1. Mesh-independent analysis.

	Number of elements	Max ANSYS Skewness	WSS point in the middle of stent wall [Pa]	% difference successive mesh densities
Mesh 1	114,812	0.871	30	
Mesh 2	2,139,088	0.846	22	30%
Mesh 3	2,646,129	0.840	21	5%

As it is shown in Fig.3, a mesh refinement is applied in the stent struts and in the stent neighboring region in order to reduce the truncation error and to capture the detailed flow features at the stent position.

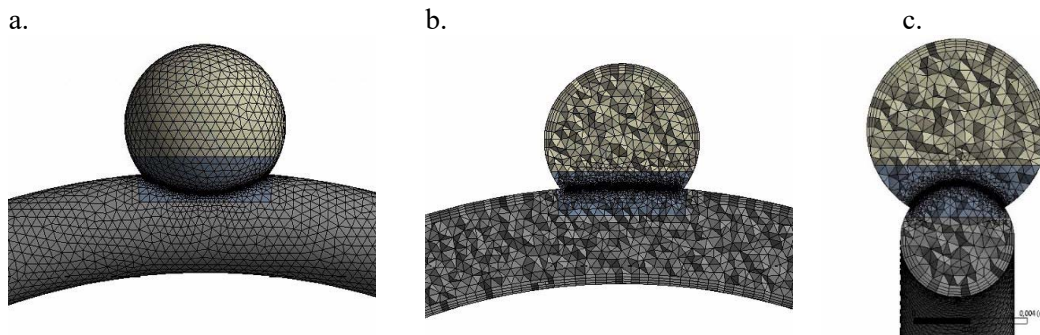


Fig.3. Mesh characteristics used in the simulation: a. surface mesh; b. mid plane section at XY plane; c. mid plane section at YZ plane.

Boundary and initial conditions

After conducting a careful literature review about steady state blood simulations, it is decided to specify a uniform inflow velocity of $0.7m/s$ as the inlet boundary condition. The outlet pressure is chosen as a reference pressure, which is defined as $0Pa$ [33, 34]. The blood flow is assumed steady, non-Newtonian and fully developed prior to particle injection. Blood and particle material details are described in Table 2.

For the continuous phase, a no-slip and rigid condition is specified at the vessel and stent walls of the computational model. In order to count the number of captured particles, a stick wall boundary condition is set at the stent wall when solving for the Lagrangian particle phase [35]. In addition, particles are free to rebound when hitting vessel walls; it is accomplished by setting a reflect wall boundary condition. Particles are allowed to escape the computational domain at inlet and outlet boundaries.

A single injection of 14520 identical non-interacting magnetic particles is set at the inlet boundary. One-way coupling interaction is enabled between the continuous phase (blood) and the particles. Due to dilute flow, interaction between particles is neglected.

Table 2. Blood and particle material details.

Symbol	Parameter	Numerical value
ρ	blood density	1050 kg/m ³
μ_o	magnetic permeability of vacuum	$4\pi \times 10^{-7} Hm^{-1}$
D_p	particle diameter	$1 \times 10^{-5} m$
ρ_p	labeled particle density	1060.7 Kg/m ³

2.4. Factors of incidence over the magnetic particle targeting efficacy

A design of experiments (DOE) factorial design 2^3 with probability value of p-value < 0.05 is proposed. Statistical significance is determined via one-way ANOVA with Statistical Software Minitab 17.0 [36]. The independent variable to be studied is the capture efficiency in the stent region.

Each possible combination of the magnetic field strength, frequency and direction with parameters described in Table 3 are evaluated, resulting in 8 different simulations. Fig.4 shows the MR scanner available options and the different magnetic field configurations. The magnetic field variation while particles are in motion is neglected.

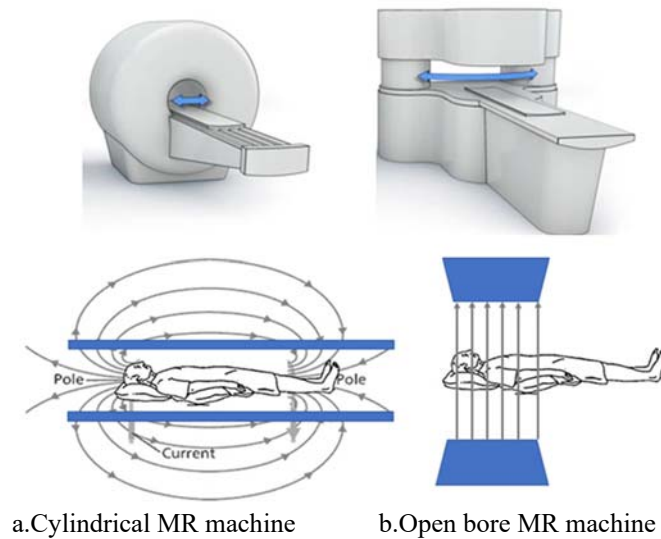


Fig.4 MR scanner configurations.

Table 3. Magnetic field strength, frequency and direction at high and low magnitudes evaluated in the study.

	Amplitude	Direction	Frequency
High Level	1 Tesla	Y – corresponding to an open bore MRI machine	AC= electromagnetic
Low Level	0.5 Tesla	(-Z) - corresponding to a cylindrical MRI machine	DC = permanent magnet

3. Results and discussion

The influence of magnetic configuration on the magnetic particles targeting efficacy is calculated in aneurysm ostium, where the stent is located. Fig.5 shows the middle line crossing the ostium, that indicates the middle point for each strut of the stent and also represents the line where the blood flow is expected to have the highest velocity at the entrance of the aneurysmal sac. Velocity across this line is calculated for each model and compared in Fig.6.

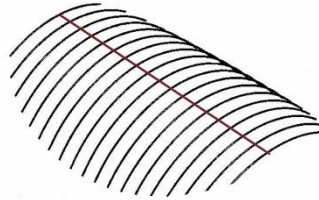


Fig.5. Ostium line.

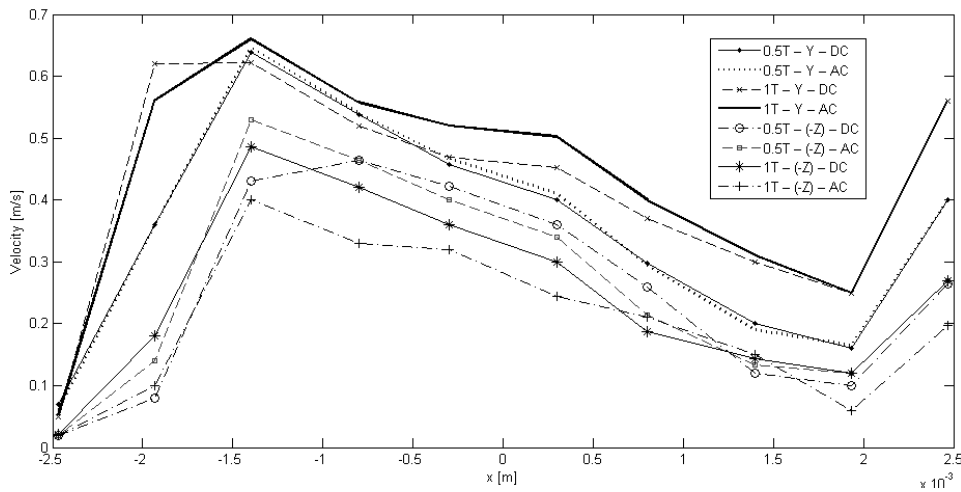


Fig.6. Velocity comparison in ostium line.

3.1. Capture efficiency

Table 4 presents the number of trapped particles and the corresponding capture efficiency for each simulation. The results presented in this table are further used for the statistical analysis. The results are compared with those of a non-magnetic field model. When the magnetic field is off, just one particle is trapped at the stent wall, which corresponds to 0.007% capture efficiency.

It can be noticed from Table 4 that the highest target efficiency is obtained for a magnetic field amplitude of 1T in an open bore MRI scanner with permanent magnet, and the lowest capture efficiency is found on a cylindrical MRI scanner with 0.5T magnetic field amplitude, when the domain is under an electromagnetic magnet.

The statistical analysis compares the mean response values at different levels of the amplitude, direction and frequency of the magnetic field and determines statistical incidence over the number of trap particles. The DOE results with an α of 0.05 and a p-value (0.001) provides enough evidence to conclude that the direction of the magnetic field is statistically significant for the capture efficiency. As presented in Fig.7, a Pareto chart is used to represent the capture efficiency among the 8 magnetic field configurations studied. A direct

effect on the preferential direction of the CE is found. The first four bars in Fig.7, that represent the highest number of trapped particles, are obtained when the magnetic field is aligned with the Y direction. This configuration corresponds to an open bore MRI machine.

Table 4. Number of trapped particles and capture efficiency.

Model	Amplitude	Direction	Frequency	# of Trapped particles	Capture Efficiency
1	1T	Y	DC	12696	87.43%
2	1T	(-Z)	DC	5383	37.07%
3	0.5T	Y	DC	10187	70.16%
4	0.5T	(-Z)	DC	3848	26.50%
5	1T	Y	AC	11097	76.43%
6	1T	(-Z)	AC	1409	9.70%
7	0.5T	Y	AC	10828	74.57%
8	0.5T	(-Z)	AC	688	4.74%

Computational results reported in this work help to improve the fundamental understanding of the hemodynamics changes in stented aneurysm under different clinical configurations that are currently in use to generate external magnetic fields. The results promote the hemodynamics-based predictions of treatment outcomes from novel treatment strategies that could impact patient outcomes.

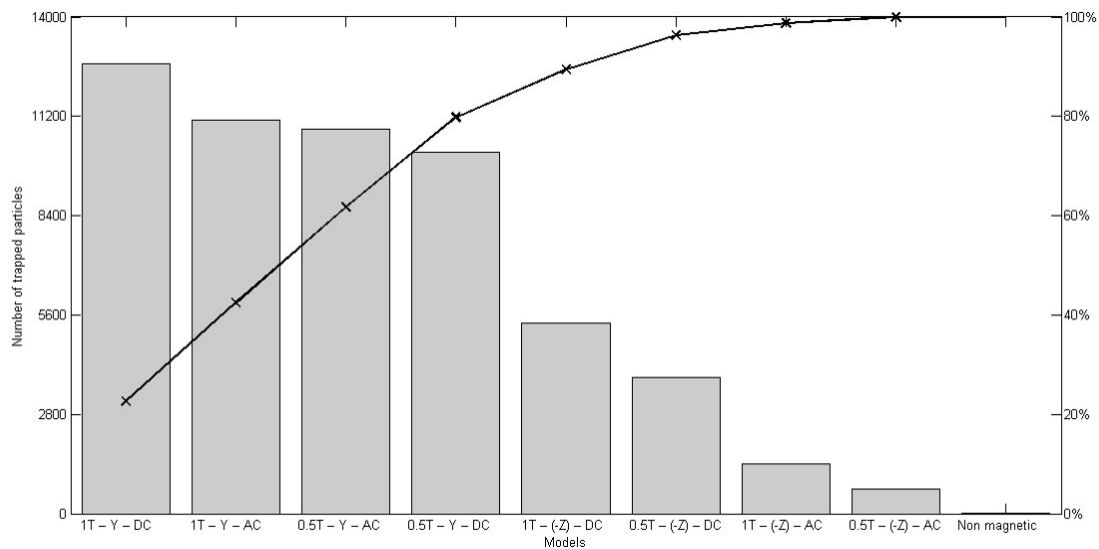


Fig.7. Pareto chart of the effects.

In concordance with the investigation by Wang *et al.* [37], in which the capture efficiency under magnetic fields with different amplitudes is evaluated, the results presented in this work show that the capture efficiency increases with a larger magnetic field strength, indicating a more significant impact of a magnetic force on particle motion with a larger magnetic field strength. It is also shown that the direction of the magnetic field has a greater incidence on the particle capture efficiency. It is shown that particle retention is greater in an open bore MRI scanner. This can be explained by stent position; as soon as the particles are injected, they are pushed to the ostium and are trapped by the struts wall. This finding corresponds with results presented by Cherry *et al.* [38] who identified that particle retention increased when the magnetic field was applied in a cross-stream direction contrary to a magnetic field oriented streamwise.

After comparing the two different magnetic field frequency alternatives, large permanent magnets and electromagnetic MRI devices, any incidence is clearly detected.

In an attempt to simulate realistic conditions, the hemodynamics is simulated using a curved representation of the vessel with an idealized saccular aneurysm. In addition, the simulated magnetic directions correspond to physically possible configurations. Still, as previously described, several assumptions and simplifications need to be done in order to reduce the computational cost.

4. Conclusions

A computational study of the blood flow in an idealized three-dimensional model of a saccular brain aneurysm is presented. A Lagrangian approach is used to track the motion of magnetically labeled particles. This study represents the first time that a factorial design has been applied to characterize the effect of amplitude, frequency and direction of the magnetic field applied to the region of interest over the magnetic particle targeting efficacy in a wide neck treated saccular brain aneurysm geometry.

It is found that the magnetic field direction affects the particle concentration in the target region. Simulation results show that the highest particle capture efficiency is obtained with a IT magnetic field amplitude when a permanent magnet is used on an open bore MRI.

The numerical model puts in evidence the crucial aspects of the flow field from the point of view of the particle accumulation in the targeted region. To have a better understanding of the phenomenon, other factors should be examined such as the effect of magnetizable stents and the interaction among magnetic particles.

Nomenclature

\vec{B}	– magnetic flux density
D	– diameter
D_p	– particle diameter
\vec{E}	– electric field
F_s	– drag force
F_m	– magnetic force
\vec{H}	– applied magnetic field
\vec{J}	– current intensity
k	– consistency index
L	– length
\vec{M}	– magnetization
n	– power-law index
p	– pressure
t	– time
\vec{V}	– flow velocity
$\dot{\gamma}$	– strain shear rate
η	– shear blood viscosity
μ	– dynamic viscosity
μ_o	– magnetic permeability of vacuum
ρ	– density
ρ_p	– labeled particle density
σ	– electric conductivity
τ_o	– yield stress threshold

5. References

- [1] Cai W., Hu C., Gong J. and Lan Q. (2018): *Anterior communicating artery aneurysm morphology and the risk of rupture.*– World Neurosurgery, vol.109, pp.119-126.
- [2] Brain Aneurysm Foundation (2018): *Brain aneurysm statistics and facts – brain aneurysm foundation.*– available online: <http://www.bafound.org/about-brain-aneurysms/brain-aneurysm-basics/brain-aneurysm-statistics-and-facts/>.
- [3] Daou B. and Jabbour P. (2016): *Flow diversion for treating middle cerebral artery aneurysms.*– World Neurosurgery, vol.90, pp.627-629.
- [4] Kutikhin A.G., Sinitsky M.Y., Yuzhalin A.E. and Velikanova E.A. (2018): *Shear stress: an essential driver of endothelial progenitor cells.*– J. Mol. Cell. Cardiol., vol.118, pp.46-69.
- [5] Marosfoi M., Langan E.T., Strittmatter L., van der Marel K., Vedantham S., Arends J., Lylyk I.R., Loganathan S., Hendricks G.M., Szikora I., Puri A.S., Wakhloo A.K. and Gounis M.J. (2016): *In situ tissue engineering: endothelial growth patterns as a function of flow diverter design.*– J. Neurointerv. Surg, vol.34, No.1, pp.16-17.
- [6] Allain J.P., Reece L., Yang Z., Armonda R., Kempaiah R. and Tigno T. (2013): *System and stent for repairing endovascular defects and methods of use.*– WO2013052934 A3, CA2851264A1, EP2763710A2, EP2763710A4, US20140277354, WO2013052934A2, p.30.
- [7] Connell J.J., Patrick P.S., Yu Y., Lythgoe M.F. and Kalber T.L. (2015): *Advanced cell therapies: targeting, tracking and actuation of cells with magnetic particles.*– Regen. Med., vol.10, No.6, pp.757-772.
- [8] Calero M., Gutiérrez L., Salas G., Luengo Y., Lázaro A., Acedo P., Morales P., Miranda R. and Villanueva A. (2014): *Efficient and safe internalization of magnetic iron oxide nanoparticles: Two fundamental requirements for biomedical applications.*– Nanomedicine Nanotechnology, Biol. Med., vol.10, No.4, pp.733-743.
- [9] Arias S.L., Shetty A.R., Senpan A., Echeverry-Rendón M., Reece L.M. and Allain J.P. (2016): *Fabrication of a functionalized magnetic bacterial nanocellulose with iron oxide nanoparticles.*– J. Vis. Exp., No.111, doi:10.3791/52951.
- [10] Gregory-Evans K., Bashar A. E. and Laver C. (2013): *Use of magnetism to enhance cell transplantation success in regenerative medicine.*– Regen. Med., vol.8, No.1, pp.1-3.
- [11] Sharma S., Singh U. and Katiyar V.K. (2015): *Magnetic field effect on flow parameters of blood along with magnetic particles in a cylindrical tube.*– J. Magn. Magn. Mater., vol.377, pp.395–401.
- [12] Songsaeng D., Geibprasert S., ter Brugge K. G., Willinsky R., Tymianski M. and Krings T. (2011): *Impact of individual intracranial arterial aneurysm morphology on initial obliteration and recurrence rates of endovascular treatments: a multivariate analysis.*– J. Neurosurg., vol.114, No.4, pp.994-1002.
- [13] Selimovic A., Ventikos Y. and Watton P. N. (2014): *Modelling the evolution of cerebral aneurysms: biomechanics, mechanobiology and multiscale modelling.*– Procedia IUTAM, vol.10, pp.396-409.
- [14] Lunnoo T. and Puangmali T. (2015): *Capture efficiency of biocompatible magnetic nanoparticles in arterial flow: a computer simulation for magnetic drug targeting.*– Nanoscale Res. Lett., vol.10, No.1., DOI: 10.1186/s11671-015-1127-5.
- [15] Bose S. and Banerjee M. (2015): *Magnetic particle capture for biomagnetic fluid flow in stenosed aortic bifurcation considering particle-fluid coupling.*– J. Magn. Magn. Mater., vol.385, pp.32-46.
- [16] Sharma S., Singh U. and Katiyar V.K. (2015): *Modeling and in vitro study on capture efficiency of magnetic nanoparticles transported in an implant - assisted cylindrical tube under magnetic field.*– Microfluid. Nanofluidics, vol.19, pp.1061-1070.
- [17] Mirzababaei S.N., Gorji T.B., Baou M., Gorji-Bandpy M. and Fatourae N. (2017): *Investigation of magnetic nanoparticle targeting in a simplified model of small vessel aneurysm.*– J. Magn. Magn. Mater., vol.426, pp.126-131.
- [18] Overweg J. (2008): *MRI main field magnets.*– Phys, vol.38, pp.25-63.
- [19] Larsen K., Cheng C., Tempel D., Parker S., Yazdani S., den Dekker V.K., Houtgraaf J.H., de Jong R., Swager-ten Hoor S., Ligtenberg E., Hanson S.R., Rowland S., Kolodgie F., Serruys P.W., Virmani R. and Duckers H.J. (2012): *Capture of circulatory endothelial progenitor cells and accelerated re-endothelialization of a bio-engineered stent in human ex vivo shunt and rabbit denudation model.*– Eur. Heart J., vol.33, No.1, pp.120-128.

- [20] Bose S. and Banerjee M. (2015): *Effect of non-Newtonian characteristics of blood on magnetic particle capture in occluded blood vessel.*– J. Magn. Magn. Mater., vol.374, pp.611-623.
- [21] Pourmehran O., Rahimi-Gorji M., Gorji-Bandpy M. and Gorji T.B. (2015): *Simulation of magnetic drug targeting through tracheobronchial airways in the presence of an external non-uniform magnetic field using Lagrangian magnetic particle tracking.*– J. Magn. Magn. Mater., vol.393, pp.380-393.
- [22] Sharma S. , Katiyar V.K. and Singh U. (2015): *Mathematical modelling for trajectories of magnetic nanoparticles in a blood vessel under magnetic field.*– J. Magn. Magn. Mater., vol.379, pp.102-107.
- [23] Adamo R.F., Fishbein I., Zhang K., Wen J., Levy R.J., Alferiev I.S., Chorny M. (2016): *Magnetically enhanced cell delivery for accelerating recovery of the endothelium in injured arteries.*– J. Control. Release, vol.222, pp.169-175.
- [24] Majee S. and Shit G.C. (2017): *Numerical investigation of MHD flow of blood and heat transfer in a stenosed arterial segment.*– J. Magn. Magn. Mater., vol.424, pp.137-147.
- [25] Haghdel M. , Kamali R. , Haghdel A. and Mansoori Z. (2017): *Effects of non-Newtonian properties of blood flow on magnetic nanoparticle targeted drug delivery.*– Nanomedicine Journal, vol.4, No.2, pp.89-97.
- [26] Valencia A. , Morales H. , Rivera R. , Bravo E. and Galvez M. (2008): *Blood flow dynamics in patient-specific cerebral aneurysm models: the relationship between wall shear stress and aneurysm area index.*– Med. Eng. Phys., vol.30, No.3, pp.329-40.
- [27] Boldock L. (2017): *The Influence of Stent Geometry on Haemodynamics and Endothelialisation.*– PhD thesis, The University of Sheffield, uk.bl.ethos.733601.
- [28] Furlani E.J. and Furlani E.P. (2007): *A model for predicting magnetic targeting of multifunctional particles in the microvasculature.*– J. Magn. Magn. Mater., vol.312, No.1, pp.187-193.
- [29] B.D. Plouffe, S.K. Murthy, and L.H. Lewis,(2015): *Fundamentals and application of magnetic particles in cell isolation and enrichment: A review.*– Reports Prog. Phys., vol.78, No.1, p.016601, doi:10.1088/0034-4885/78/1/016601.
- [30] Xu J, Wu Z., Yu Y., Lv N., Wang S., Karmonik C., Liu J.-M. and Huang Q. (2015): *Combined effects of flow diverting strategies and parent artery curvature on aneurysmal hemodynamics: a CFD study.*– PLoS One, vol.10, No.9, p.e0138648.
- [31] Bouillot P., Brina O., Ouared R., Yilmaz H., Lovblad K.-O., Farhat M. and Pereira V.M. (2016): *Computational fluid dynamics with stents: quantitative comparison with particle image velocimetry for three commercial off the shelf intracranial stents.*– J. Neurointerv. Surg., vol.8, No.3, pp.309-15.
- [32] ANSYS Inc. (2013): *ANSYS® Academic Research Mechanical.*– ANSYS, Inc. Private communications.
- [33] Zarrinkoob L., Ambarki K., Wählin A., Birgander R., Eklund A. and Malm J. (2015): *Blood flow distribution in cerebral arteries.*– J. Cereb. Blood Flow Metab., vol.35, No.4, pp.648-654, .
- [34] Lopez Ramirez E. (2011): *Numerical Investigation of Blood Flow in Stented Intracranial Aneurysms Models.*– PhD. Thesis, Friedrich-Alexander-Universität Erlangen-Nürnberg (FAU).
- [35] Fluent A. (2001): *Chapter 19. Discrete Phase Models.*– FLUENT User's Guide. pp.1-170.
- [36] Minitab (2018): Minitab.– Pennsylvania.
- [37] Wang S., Zhou Y., Tan J., Xu J., Yang J. and Liu Y. (2014): *Computational modeling of magnetic nanoparticle targeting to stent surface under high gradient field.*– Comput. Mech., vol.53, No.3, pp.403-412.
- [38] Cherry E.M. and Eaton J.K. (2014): *A comprehensive model of magnetic particle motion during magnetic drug targeting.*– Int. J. Multiph. Flow, vol.59, pp.173-185.

Received: August 8, 2020

Revised: January 2, 2021